Hindawi
Journal of Robotics
Volume 2024, Article ID 9809817, 1 page
https://doi.org/10.1155/2024/9809817

Retraction

Retracted: Application of Intelligent Signal Reflection in the Communication Model of an Electronic Controller

Journal of Robotics

Received 23 January 2024; Accepted 23 January 2024; Published 24 January 2024

This article has been retracted by Hindawi following an investigation undertaken by the publisher [1]. This investigation has uncovered evidence of one or more of the following indicators of systematic manipulation of the publication process:

(1) Discrepancies in scope
(2) Discrepancies in the description of the research reported
(3) Discrepancies between the availability of data and the research described
(4) Inappropriate citations
(5) Incoherent, meaningless and/or irrelevant content included in the article
(6) Manipulated or compromised peer review

The presence of these indicators undermines our confidence in the integrity of the article's content and we cannot, therefore, vouch for its reliability. Please note that this notice is intended solely to alert readers that the content of this article is unreliable. We have not investigated whether authors were aware of or involved in the systematic manipulation of the publication process.

Wiley and Hindawi regrets that the usual quality checks did not identify these issues before publication and have since put additional measures in place to safeguard research integrity.

We wish to credit our own Research Integrity and Research Publishing teams and anonymous and named external researchers and research integrity experts for contributing to this investigation.

The corresponding author, as the representative of all authors, has been given the opportunity to register their agreement or disagreement to this retraction. We have kept a record of any response received.

References

[1] L. Lan, "Application of Intelligent Signal Reflection in the Communication Model of an Electronic Controller," *Journal of Robotics*, vol. 2022, Article ID 8031024, 9 pages, 2022.

Hindawi
Journal of Robotics
Volume 2022, Article ID 8031024, 9 pages
https://doi.org/10.1155/2022/8031024

Research Article

Application of Intelligent Signal Reflection in the Communication Model of an Electronic Controller

Lan Lan

Henan College of Transportation, Zhengzhou, Henan 450000, China

Correspondence should be addressed to Lan Lan; lanxin112@126.com

Received 25 August 2022; Revised 19 September 2022; Accepted 27 September 2022; Published 12 October 2022

Academic Editor: Shahid Hussain

This paper analyses the automatic control effect of an electronic controller, combined with artificial intelligence technology in order to improve the automatic control of an electronic controller. In order to improve the automatic control effect of the electronic controller, a novel centralized intelligent reflective surface-assisted millimeter-wave computational imaging scheme based on pixel block division and block sparse signal recovery is proposed in this paper. Meanwhile, this paper proposes a fast block-sparse Bayesian learning algorithm. It combines the GAMP algorithm with machine learning, so it can achieve similar performance with much lower computational complexity than the traditional block sparse Bayesian learning algorithm. The simulation clustering study shows that the electronic controller automation system based on artificial intelligence technology proposed in this paper can effectively improve the control effect of the electronic controller.

1. Introduction

Since the beginning of the twenty-first century, electronic technology, especially microelectronics technology, has been changing with each passing day, and the performance requirements of automobiles are also becoming more stringent [1]. The rapid development of the automotive market has also driven the continuous advancement of body control systems. At present, the original distributed body control system is being eliminated from the market, and products are developing from the centralized body control system to the distributed body control system [2]. A body control system (BCM) refers to the automotive electrical system in which a controller is responsible for monitoring and controlling all electrical equipment in the vehicle body. Usually, the body control system is responsible for controlling the door and window lifts, electric rear view mirrors, air conditioning, central locking, and antitheft password systems. At the same time, the body control system can communicate with other controllers through various automobile buses [3]. The development trend of the future body control system is digital, intelligent, and networked. Connecting various electrical devices and control units through the bus can simplify the wiring harness layout of the whole vehicle, facilitate the expansion of future system functions, and reduce the weight of the vehicle wiring harness. At the same time, the diagnosable function is also conducive to the inspection and maintenance of the car. The driver can easily understand the working status of each system of the car through the display of the combination instrument before starting, so as to ensure the safety of the car [4]. The maintenance personnel can quickly determine the specific location of the fault by reading the fault information through the fault diagnosis instrument, which reduces the difficulty of troubleshooting and reduces the maintenance time [5]. At the same time, the car bus can realize information sharing and cooperative work between different electrical systems, laying the foundation for greater car intelligence in the future.

The centralized body control system means that multiple body electrical subsystems are controlled centrally through one controller. All switches and sensors are connected to the same controller. A certain logical relationship can occur between each body's electrical subsystem, and at the same time, through the bus connection, a certain logical relationship can occur between the body control system and the

power system and even the entertainment system, air conditioning system, and instrumentation system, such as the alarm of the air conditioning system. The main controller component of the centralized system is the body controller (BCM), which is the core of the centralized body control system [6]. The body controller can be further divided into a bus-type body controller and a non-bus-type body controller. The bus-type body control system can simultaneously function as a gateway. The aforementioned CBCU is a centralized body control system [7].

The centralized body control system greatly strengthens the control functions of humanization, comfort, and safety, and the fault diagnosis of the electric equipment of the whole vehicle is also simplified. Reasonable use, under the premise of the same technical requirements, can reduce the overall cost of the body control system [8]. Of course, there are downsides to centralized body control systems. Compared with the distributed system, the development of the body controller is more difficult, especially in terms of the software structure of the controller and the reliability of the system; since many electrical devices are controlled by one controller, when the configuration of the vehicle electrical system changes a lot, the centralized body control system tends to exist in many states, requiring a lot of repeated development and testing. Redundant development will result in a waste of resources, and the cost is not easy to control [9].

In terms of form, the distributed body control system is similar to the decentralized system in that each subsystem of the body electrical appliances is controlled by a separate controller, but there are great differences in essence. There is no relationship between the electrical appliances of the distributed body control system and the distributed body control system inherits the advantages of the centralized body control system in functional control. In addition to the logic control, it also communicates through the bus to realize the functional interaction of various areas and subsystems, such as body appliances, power systems, entertainment systems, and instrumentation systems [10]. In the distributed body control system, the communication of all control modules becomes very critical, and the realization of almost all control functions is inseparable from the existence of communication [11]. For example, in a centralized control system, all door lock motors are directly driven by the body controller, while in a distributed system, each door control module first obtains a lock and unlock signal through the bus, and then each door control module independently drives each door lock motor. When OEMs use the distributed body control system, they should define the basic bus protocol, all messages and their reasonable attributes (message sending method, period, signal meaning, etc.), network management methods, diagnosis according to the system functional requirements, protocol, etc. and formulate strict test specifications and complete the test software design to ensure that the communication effect of the bus meets the functional requirements [12].

With the rapid development of Internet services, network management has become more and more complex on the existing network architecture, and it is difficult for researchers to conduct new innovative experiments. In order to simplify network management and reduce the difficulty for researchers to conduct innovative experiments, a new network architecture of software defined networking (SDN) is proposed, which decouples the control plane and data plane of network devices [12], so that network administrators can easily manages network services flexibly and conveniently and, at the same time, cooperate with the OpenFlow protocol, making it easier for researchers to conduct innovative network experiments. The emergence of SDN quickly attracted the attention of a large number of enterprises, such as equipment manufacturers, telecom operators, and Internet companies. Compared with the existing network, SDN can improve the intelligent forwarding capability of the network edge, make the deployment and upgrade of network equipment more convenient, and improve the network's open capability [13]. As the middle layer of the SDN architecture, the SDN controller, on the one hand, opens network programming capabilities to the application layer through the northbound interface, so that the application layer does not need to care about specific details and has the ability to control network behavior; the underlying network equipment is managed and dispatched in a unified manner. It is a bridge connecting the infrastructure layer and the application layer and has an important position as a "network operating system" [14]. In recent years, with the development and maturity of SDN, many enterprises have begun to commercialize SDN deployment, and various open-source controllers have been developed one after another. However, there are still many deficiencies in the research work on the performance testing of SDN controllers in the industry. For example, the test content of the SDN controller performance test is not comprehensive enough; there are few open-source test tools, and most of the test tools can only simulate independent switches for testing but cannot form the topology between switches [15]. Most of the open source testing tools do not support testing controller clusters; therefore, it is difficult for the existing open-source test tools to make a comprehensive evaluation of the performance of the SDN controller, which is unfavorable for the further development of the SDN controller, and the SDN controller is the core component of the SDN architecture which hinder the development of SDN [16].

Any network is in constant change, and so is an SDN network. In the SDN network, when the network changes, for example, a new switch is turned on/off, the switch port is turned on/off, the switch needs to send a specific message to the SDN controller to notify the SDN controller that the network has changed, and the SDN control The response time of the SDN controller to such messages reflects the sensitivity of the SDN controller to network changes and determines whether the SDN controller can perceive network changes in a timely manner [17]. Four indicators are added to the test system to test the response time of the SDN controller to topology events. In an SDN network, since the SDN controller is the brain of the entire network, when the switch encounters a packet that cannot be

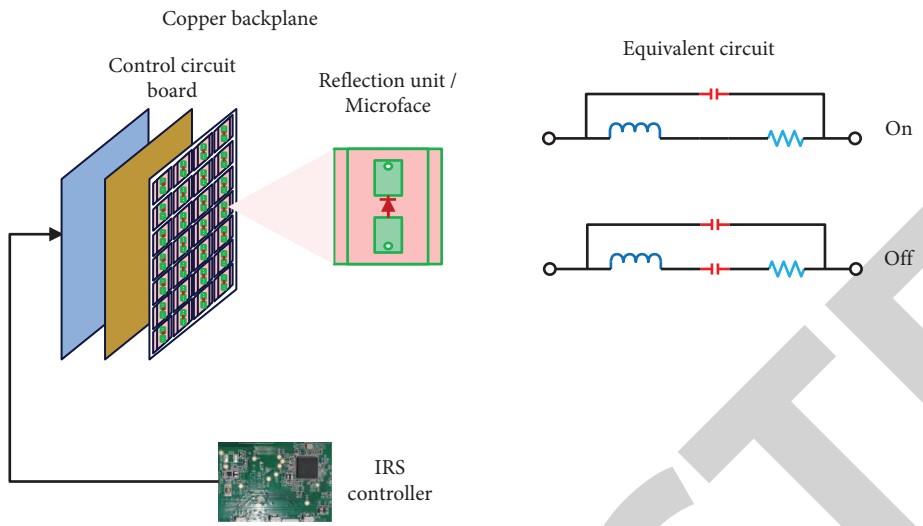

Figure 1: The hardware architecture of the smart reflector.

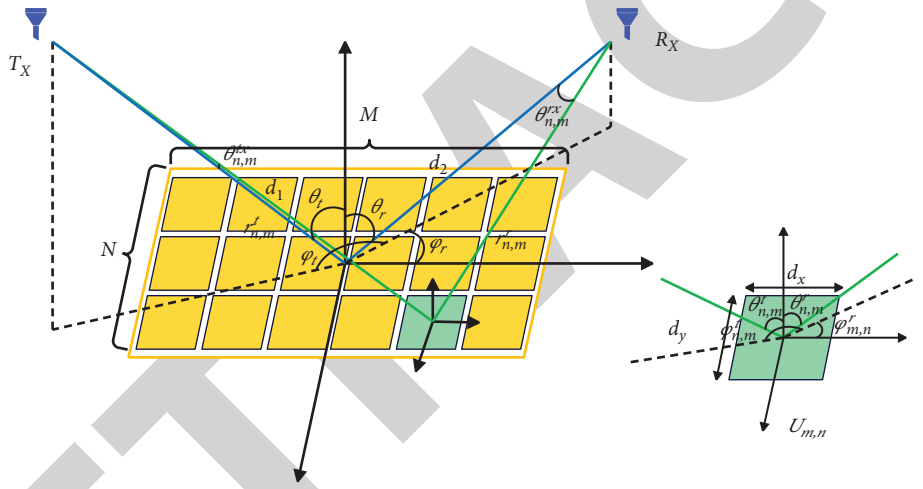

Figure 2: Physical model of the smart reflector.

processed, it will send a request to the SDN controller, and then the SDN controller decides how to process the packet. The processing speed of the SDN controller, that is, the response time, affects the transmission efficiency of data packets in the SDN network, which is of great significance [18]. The end-to-end path establishment time indicator is to test this capability of the SDN controller. The end-to-end path establishment time indicator not only tests the processing time of the SDN controller for a packet request but also tests the sum of the processing times of the SDN controller for each switch on a complete path, which is more suitable. realistic scene. Therefore, we chose the end-to-end path setup time metric as a metric for the SDN controller response time class.

This paper combines artificial intelligence technology to analyze the automatic control of the electronic controller and constructs an automatic control system for the electronic controller based on the artificial intelligence technology to promote the intelligent application effect of the electronic controller.

2. Communication Model of Electronic Controller Based on Intelligent Reflector

2.1. Smart Reflector. As shown in Figure 1, the typical architecture of the IRS consists of three layers and an intelligent controller. The physical model of the smart reflector when it reflects the signal is shown in Figure 2. The area of each microfacet on the IRS is $d_x \times d_y$, where d_x and d_y are the side lengths along the x-axis and y-axis, respectively, and their sizes are generally between $\lambda/10$ and $\lambda/2$. G is the gain of the microfacet, which is defined as

$$G = \frac{4\pi}{\int_{\phi=0}^{2\pi}\int_{\theta=0}^{\pi} F(\theta,\phi)\sin\theta \mathrm{d}\theta\mathrm{d}\phi}. \quad (1)$$

It is only related to the normalized power pattern $F(\theta,\phi)$ of the microfacet.

The power of the signal incident on a single microfacet $U_{n,m}$ can be expressed as

$$P_{n,m}^{in} = \frac{G_t P_t}{4\pi\left(r_{n,m}^t\right)^2} F^{tx}\left(\theta_{n,m}^{tx}, \phi_{n,m}^{tx}\right) F\left(\theta_{n,m}^t, \phi_{n,m}^t\right) d_x d_y. \quad (2)$$

The electric field of the incident signal to $U_{n,m}$ is

$$E_{n,m}^{in} = \sqrt{\frac{2Z_0 P_{n,m}^{in}}{d_x d_y}} e^{\left(-j2\pi r_{n,m}^t\right)/(\lambda)}. \quad (3)$$

Among them, Z_0 is the characteristic impedance of air, and $r_{n,m}^t$ can be written as

$$r_{n,m}^t = \sqrt{\left(x_t - \frac{2m-1}{2} d_x\right)^2 + \left(y_t - \frac{2n-1}{2} d_y\right)^2 + z_t^2}, \quad (4)$$

$$P_{n,m}^{in} \left|\Gamma_{n,m}^2\right| = P_{n,m}^{\text{reflect}}.$$

Among them, $P_{n,m}^{\text{reflect}}$ is the total power of the reflected signal of the microfacet $U_{n,m}$. The power of the reflected signal received by the receiver from $U_{n,m}$ can be expressed as

$$P_{n,m}^r = \frac{G P_{n,m}^{\text{reflect}}}{4\pi\left(r_{n,m}^r\right)^2} F\left(\theta_{n,m}^r, \phi_{n,m}^r\right) F^{rx}\left(\theta_{n,m}^{rx}, \phi_{n,m}^{rx}\right) A_r,$$

$$E_{n,m}^r = \sqrt{\frac{2Z_0 P_{n,m}^r}{A_r}} e^{-j\left(\left(2\pi r_{n,m}^t/\lambda\right) + \left(2\pi r_{n,m}^r/\lambda\right)\phi_{n,m}\right)},$$

$$= \sqrt{\frac{Z_0 P_t G_t G d_x d_y F_{n,m}^{\text{combine}}}{8\pi^2}} \frac{\Gamma_{n,m}}{r_{n,m}^t r_{n,m}^r} e^{\left(-j2\pi\left(r_{n,m}^t + r_{n,m}^r\right)\right)/\lambda}. \quad (5)$$

Among them, $F_{n,m}^{\text{combine}} = F^{tx}(\theta_{n,m}^{tx}, \phi_{n,m}^{tx}) F(\theta_{n,m}^t, \phi_{n,m}^t) F(\theta_{n,m}^r, \phi_{n,m}^r) F^{rx}(\theta_{n,m}^{rx}, \phi_{n,m}^{rx})$ represents the effect of the normalized power pattern on the received signal power. The total electric field of the received signal is the superposition of the electric fields reflected from all unit cells towards the receiver

$$E^r = \sum_{m=1-(M/2)}^{M/2} \sum_{n=1-(N/2)}^{N/2} E_{n,m^\circ}^r. \quad (6)$$

The received signal power of the receiver is

$$P_r = \frac{\left|E^r\right|^2}{2Z_0} A_r. \quad (7)$$

Among them, $A_r = (G_r \lambda^2)/(4\pi)$ is the aperture of the receive antenna. The received signal power is as follows

$$P_r = P_t \frac{G_t G_r G d_x d_y \lambda^2}{64\pi^3} \left| \sum_{m=1-(M/2)}^{M/2} \sum_{n=1-(N/2)}^{N/2} \frac{\sqrt{F_{n,m}^{\text{combine}} \Gamma_{n,m}}}{r_{n,m}^t r_{n,m}^r} e^{\left(-j2\pi\left(r_{n,m}^t + r_{n,m}^r\right)\right)/(\lambda)} \right|^2. \quad (8)$$

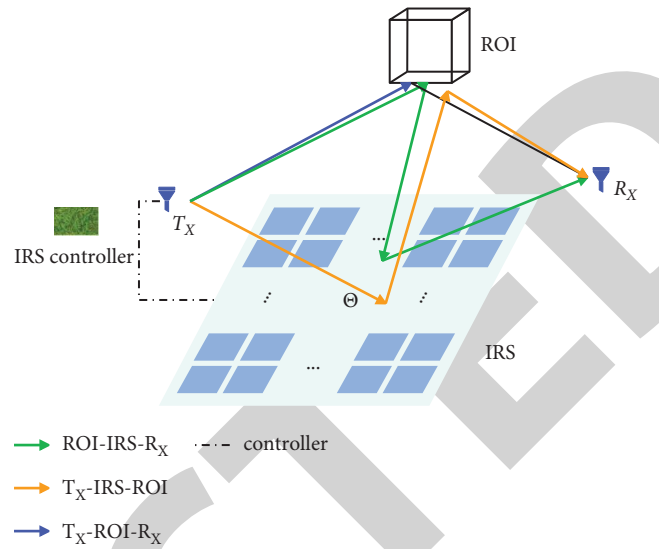

Figure 3: Imaging system model (centralized IRS mode).

2.2. System Model and Problem Description. The imaging system is shown in Figure 3. Both the transmitter (Tx) and receiver (Rx) are equipped with a single antenna for imaging and are connected to the control equipment through control lines, and the centralized IRS working mode is used here. The imaging system corresponding to the separate IRS working mode is shown in Figure 4. The IRS is connected to the control device through the IRS controller. That is, each microfacet is composed of $\overline{K}$ minimum unit faces, as shown in $\overline{K} = 4$ in Figure 4. The microfacet mentioned in the following refers to the microfacet after the combination. The three-dimensional imaging region to be detected and reconstructed in the imaging system model is called the region of imaging (ROI). The reflectance of all pixels in the ROI is represented by

$$x = \left[x_1, x_2, \ldots, x_N\right]^T \in \mathscr{C}^{N\times 1}, \quad (9)$$

we assume that the locations of T_x, R_x, IRS, and ROI are all known in advance.

It is assumed that the IRS consists of K microfacets:

$$\Theta = \text{diag}\left(\Theta_1, \ldots, \Theta_K\right) \in \mathscr{C}^{K\times K}. \quad (10)$$

Among them, $\Theta_k = \rho_k e^{j\theta_k}$ represents the reflection characteristic of the k-th microfacet of the IRS, and $\rho_k \in [0, 1]$ and $\theta_k \in [0, 2\pi]$ are diagonal matrices. If b_1 bits are used to represent the amplitude reflection coefficient, ρ

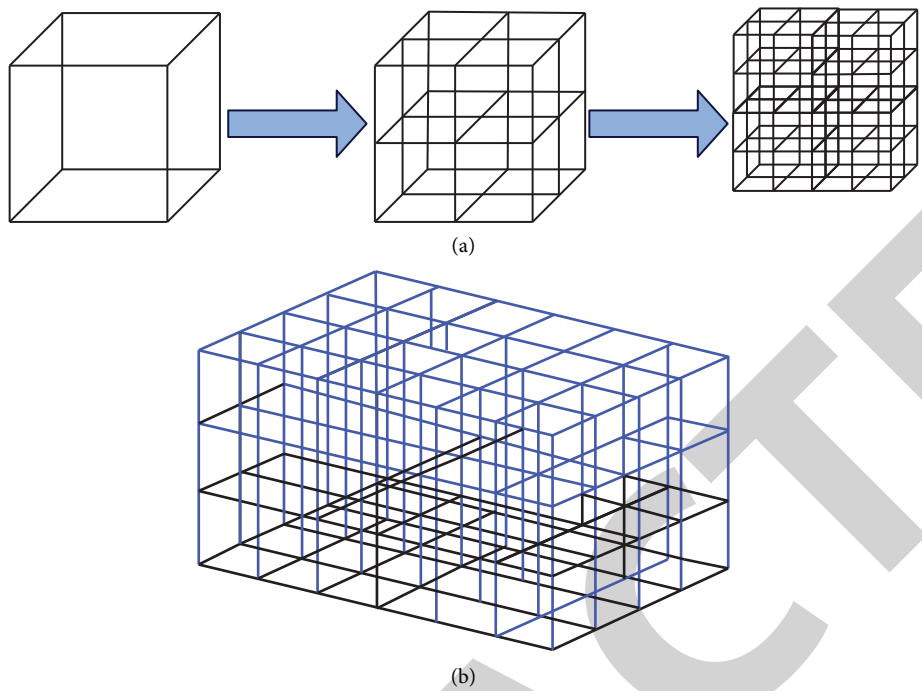

Figure 4: Pixel division method of target area. (a) Division method of the ROI. (b) An example of a target division.

has 2^{b_1} different values with uniform intervals, of which the maximum value is $\rho_{\max}$, the minimum value is $\rho_{\min}$, and the interval is $\Delta\rho = (\rho_{\max} - \rho_{\min})/(2^{b_1-1})$, that is, $\rho \in \{\rho_{\min}, \rho_{\min} + \Delta\rho, \ldots, \rho_{\max}\}$. If b_2 bits are used to represent the phase offset, then θ has 2^{b_2} different values with uniform intervals, of which the minimum value is 0 and the interval is $\Delta\theta = (2\pi)/(2^{b_2})$, that is, $\rho \in \{0, \Delta\theta, 2\Delta\theta, \ldots, (2^{b_2} - 1)\Delta\theta\}$. In the process of imaging, Θ does not always remain constant, but adjusts with time, so Θ is actually a hop function $\Theta(t)$ that changes with time.

It is assumed that all channels in the figure are constant parameter channels, that is, the influence of the channel on the signal is fixed or changes very slowly with time. Among them, the channels from Tx to ROI and IRS are $H_{TO} = [h_1^{TO}, \ldots, h_N^{TO}] \in \mathscr{C}^{1\times N}$ and $H_{TI} = [h_1^{TI}, \ldots, h_K^{TI}] \in \mathscr{C}^{1\times K}$, respectively. Among them, $h_n^{TO} = a_n^{TO} e^{i\phi_n^{TO}}$ represents the channel from Tx to the nth pixel of R0I, a_n^{TO} and ϕ_n^{TO} are the amplitude parameter and phase offset of this channel, respectively, $h_k^{TI} = a_k^{TI} e^{i\phi_k^{TI}}$ represents the channel from Tx to the k-th microfacet of IRS, and a_n^{TI} and ϕ_k^{TI} are the amplitude parameter and phase offset of the channel, respectively. The IRS and ROI to Rx channels are $H_{IR} = [h_1^{IR}, \ldots, h_K^{IR}] \in \mathscr{C}^{1\times K}$ and $H_{OR} = [h_1^{OR}, \ldots, h_N^{OR}] \in \mathscr{C}^{1\times N}$, respectively. Among them, $h_k^{IR} = a_k^{IR} e^{i\phi_k^{IR}}$ is the channel to which the k-th microfacet of the IRS to Rx, a_k^{IR}, and ϕ_k^{IR} are the amplitude characteristic and phase offset of this channel, respectively, $h_n^{OR} = a_n^{OR} e^{i\phi_n^{OR}}$ is the channel to which the nth pixel of the ROI to Rx, and a_n^{OR} and ϕ_n^{OR} are the amplitude characteristics and phase offset of this channel, respectively. The channel from IRS to ROI is the channel of H_{IO} = pixels, and $a_{k,n}^{IO}$ and $\phi_{k,n}^{IO}$ are the amplitude characteristics and phase offset of this channel, respectively. It is assumed that the channel from IRS to ROI and the channel from ROI to IRS are the same.

If it is assumed that the transmitted signal is (t), the received signal of the subchannel from Tx to the nth pixel of ROI and then to Rx is

$$y_n^{\mathrm{TOR}}(t) = a_n^{TO} e^{i\phi_n^{TO}} x_n a_n^{OR} e^{i\phi_n^{OR}} s(t) = x_n h_n^{\mathrm{TOR}} s(t). \tag{11}$$

Among them, $h_n^{TOR} = a_n^{TO} a_n^{OR} e^{i\phi_n^{TO}} e^{i\phi_n^{OR}}$ is the subchannel at $x_n = 1$. The received signal from the sub-channel Tx to the k-th microfacet of the IRS to the nth pixel of the ROI and finally to Rx is

$$\begin{aligned} y_{n,k}^{\mathrm{TIOR}}(t) &= a_k^{TI} e^{i\phi_k^{TI}} \rho_k e^{j\theta_k} a_{k,n}^{IO} e^{i\phi_{k,n}^{IO}} x_n a_n^{OR} e^{i\phi_n^{OR}} s(t) \\ &= x_n h_{n,k}^{\mathrm{TIOR}} s(t). \end{aligned} \tag{12}$$

Among them, $h_{n,k}^{\mathrm{TIOR}} = a_k^{TI} a_{k,n}^{IO} a_n^{OR} \rho_k e^{i(\phi_k^{TI} + \theta_k + \phi_{k,n}^{IO} + \phi_n^{OR})}$ is the subchannel at $x_n = 1$. The received signal from sub-channel Tx to the nth pixel of the ROI to the k-th microfacet of the IRS to Rx is

$$\begin{aligned} y_{n,k}^{\mathrm{TOIR}}(t) &= a_n^{TO} e^{i\phi_n^{TO}} a_{k,n}^{IO} e^{i\phi_{k,n}^{IO}} x_n \rho_k e^{j\theta_k} a_k^{IR} e^{i\phi_k^{IR}} s(t) \\ &= x_n h_{n,k}^{\mathrm{TOIR}} s(t). \end{aligned} \tag{13}$$

Among them, $h_{n,k}^{\mathrm{TOIR}} = a_n^{TO} e^{i\phi_n^{TO}} a_{k,n}^{IO} e^{i\phi_{k,n}^{IO}} \rho_k e^{j\theta_k} a_k^{IR} e^{i\phi_k^{IR}}$ is the subchannel at $x_n = 1$. The total received signal received by the final receiver is

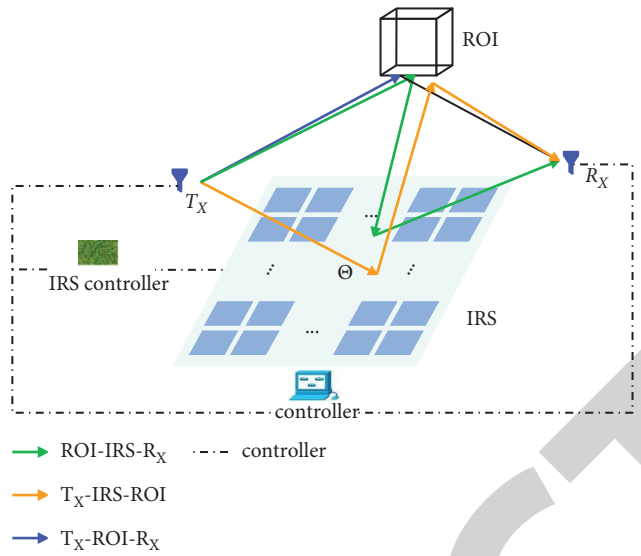

Figure 5: Schematic diagram of the use of centralized smart reflectors (separate IRS mode).

$$\begin{aligned} y(t) &= \sum_{n=1}^{N} y_n^{\mathrm{TOR}}(t) + \sum_{k=1}^{K}\sum_{n=1}^{N} y_{n,k}^{\mathrm{TIOR}}(t) + \sum_{k=1}^{K}\sum_{n=1}^{N} y_{n,k}^{\mathrm{TOIR}}(t) + w \\ &= \sum_{n=1}^{N} x_n h_n^{\mathrm{TOR}} s(t) + \sum_{k=1}^{K}\sum_{n=1}^{N} x_n h_{n,k}^{\mathrm{TIOR}} s(t) + \sum_{k=1}^{K}\sum_{n=1}^{N} x_n h_{n,k}^{\mathrm{TOIR}} s(t) \\ &\quad + w \\ &= \sum_{n=1}^{N} \left(h_n^{\mathrm{TOR}} + \sum_{k=1}^{K} h_{n,k}^{\mathrm{TIOR}} + \sum_{k=1}^{K} h_{n,k}^{\mathrm{TOIR}} \right) s(t) x_n + w \\ &= \sum_{n=1}^{N} \Phi_n(t) x_n + w. \end{aligned} \tag{14}$$

Among them, $\Phi_n(t) = (h_n^{\mathrm{TOR}} + \sum_{k=1}^{K} h_{n,k}^{\mathrm{TIOR}} + \sum_{k=1}^{K} h_{n,k}^{\mathrm{TOIR}})$ $s(t)$, $\mathbf{w}$ is additive white noise. If we assume that we use uniform sampling at the transmitter and receiver, the sampling frequency is f_s, and the duration of the transmitted signal is T, the number of sampling points is $M = Tf_S$. If uniform sampling is performed according to $t = [t_1, t_2, \ldots, t_M]^T$, we can get:

$$\begin{bmatrix} y(t_1) \\ \vdots \\ y(t_M) \end{bmatrix} = \begin{bmatrix} \Phi_1(t_1) \cdots \Phi_N(t_1) \\ \vdots \ddots \vdots \\ \Phi_1(t_M) \cdots \Phi_N(t_M) \end{bmatrix} \begin{bmatrix} x_1 \\ \vdots \\ x_N \end{bmatrix} + \mathbf{w}. \tag{15}$$

If we record $\mathbf{y} = \begin{bmatrix} y(t_1) \\ \vdots \\ y(t_M) \end{bmatrix}$, $\Phi = \begin{bmatrix} \Phi_1(t_1) \cdots \Phi_N(t_1) \\ \vdots \ddots \vdots \\ \Phi_1(t_M) \cdots \Phi_N(t_M) \end{bmatrix}$, we can get the relationship between the received signal sequence and the sequence composed of the reflection parameters of the pixels of ROI as follows

$$y = \Phi x + w, \tag{16}$$

The transmitted signal is a random frequency hopping signal, which consists of P time slots. First, the entire bandwidth B is divided into C_a subcarriers, and in each time slot, C is randomly selected as a signal carrier, and each carrier is subjected to random amplitude and phase modulation to form a transmitted signal. The transmitted signal of the p-th time slot is:

$$s_p(t) = \sum_{c=1}^{c} a_{c,p} e^{-j\omega_{c,p}t} e^{jb_{c,p}}, \ (p-1)\tau \le t \le p\tau. \tag{17}$$

Among them, $\omega_{c,p}, a_{c,p}$, and $b_{c,p}$ are the frequency, amplitude, and phase of the c-th carrier selected for this slot, respectively. Then, the final composition of the transmitted signal is

$$s(t) = \sum_{p=1}^{P} s_p(t) = \sum_{p=1}^{P}\sum_{c=1}^{c} a_{c,p} e^{-j\omega_{c,p}t} e^{jb_{c,p}}. \tag{18}$$

From the physical model of IRS, it can be known that the received signal power of the signal reaching the receiver or ROI after being reflected by the intelligent reflective surface is negatively correlated with the distance between the IRS and the position where the signal is sent/received. That is, the farther the IRS is from the location where the signal is sent/received, the smaller the received signal power will be. The performance is that in the received signal $y(t)$, the proportion of the two parts $\sum_{k=1}^{K}\sum_{n=1}^{N} y_{n,k}^{\mathrm{TIOR}}(t)$ and $\sum_{k=1}^{K}\sum_{n=1}^{N} y_{n,k}^{\mathrm{TIOR}}(t)$ passing through the IRS will decrease, and the part $\sum_{n=1}^{N} y_n^{\mathrm{TOR}}(t)$ that does not pass through the IRS will increase accordingly. Therefore, the different positions of the IRS will change the role of the IRS. Accordingly, we propose two different working modes of IRS: centralized/distributed IRS. We call the centralized IRS working mode when the distance between the IRS and the location where the signal is sent/received is close, and the distributed IRS working mode when the distance is farther. A schematic diagram of the use of centralized smart reflectors is shown in Figure 5.

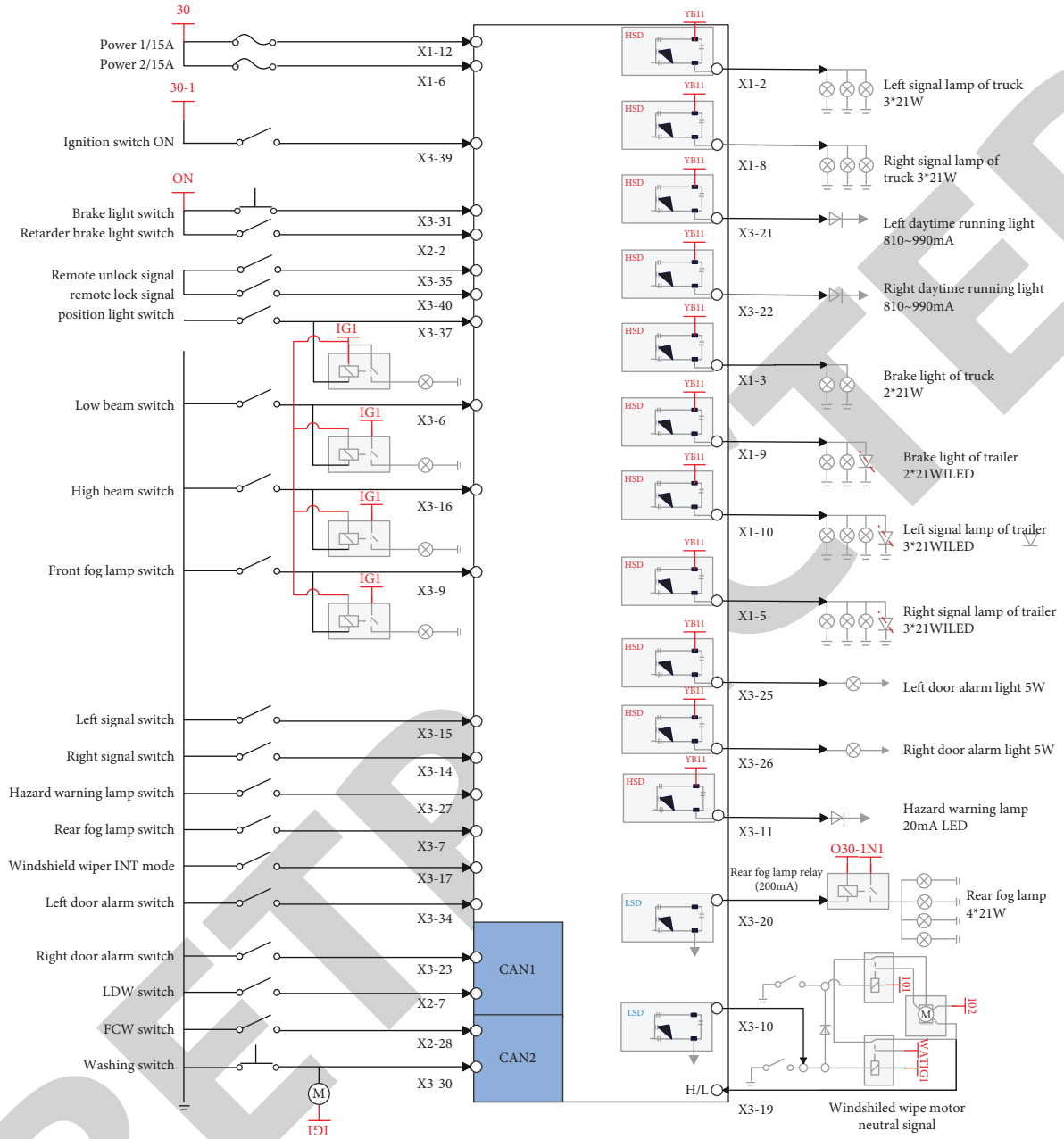

Figure 6: Schematic diagram of the body controller system.

3. Electronic Controller Automation Control System

According to the function of the body control system and the definition requirements of the peripheral input and output interfaces, the schematic diagram of the body control system is designed as shown in Figure 6.

The overall framework of the SDN controller performance test platform is designed as shown in Figure 7. As can be seen from the figure, the SDN controller performance test platform framework designed in this paper is divided into four modules, including the virtual switch module, service analysis module, test dispatch center module, and user interaction center module. The virtual switch module is mainly responsible for simulating the behavior of the switch, including establishing and maintaining the connection with the SDN controller, processing the topology request of the SDN controller, forming the corresponding topology according to the topology information configured by the user, sending and receiving test packets, etc.

The effect of the electronic controller automation system based on artificial intelligence technology proposed in this paper is verified, and the system performance is verified by cluster analysis, and the results shown in Figure 8 are obtained.

It can be seen from the above research that the electronic controller automation system based on artificial intelligence technology proposed in this paper can effectively improve the control effect of the electronic controller.

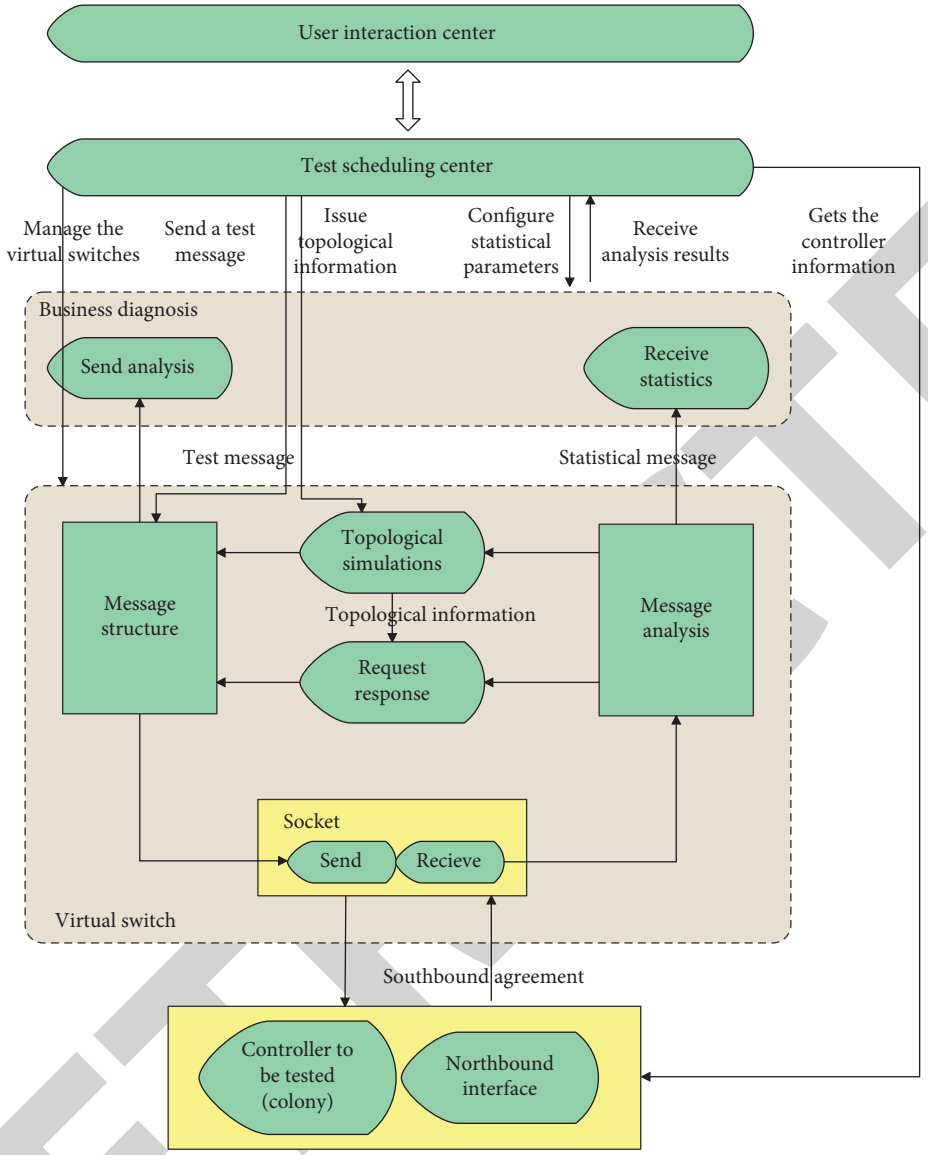

Figure 7: Frame diagram of the controller performance test platform.

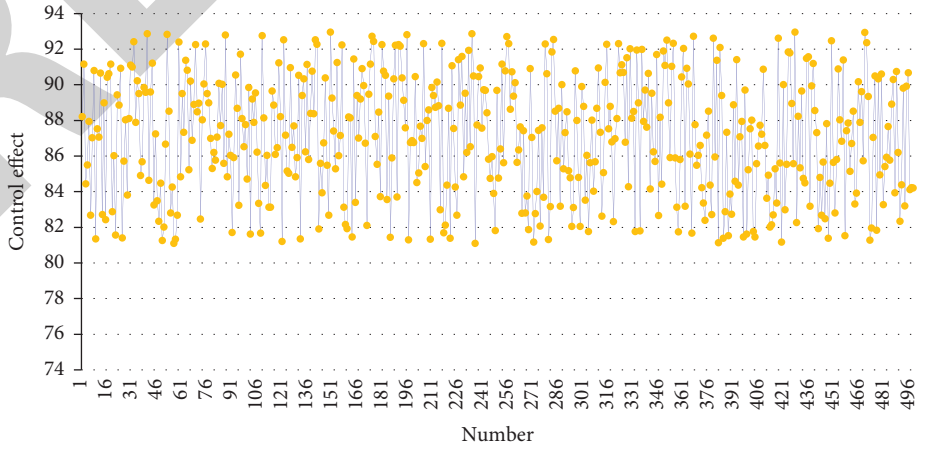

Figure 8: Verification of the effect of the electronic controller automation system based on artificial intelligence technology.

4. Conclusion

With the continuous progress of social economy and science and technology, there are more and more electrical equipment on automobiles. Moreover, consumers' requirements for the intelligence, safety, stability, and comfort of automobiles are constantly improving, and the traditional automobile electrical system can no longer meet the needs of users. Therefore, the body control system was born. The body control system is a system used to realize the humanization, comfort, and partial safety control of the body electrical equipment, including the functions of the vehicle's interior lights, wipers, central control, and lighting control. This paper analyzes the automatic control of electronic controllers combined with artificial intelligence technology and constructs an automatic control system for electronic controllers based on artificial intelligence technology. The simulation clustering study shows that the electronic controller automation system based on artificial intelligence technology proposed in this paper can effectively improve the control effect of the electronic controller [19].

Data Availability

The labeled dataset used to support the findings of this study are available from the corresponding author upon request.

Conflicts of Interest

The authors declare that there are no conflicts of interest.

Acknowledgments

This work was supported by the Henan Province Education Science Fifteen Planning Project 5G era School-Enterprise Education Intelligent Transportation (E+N) Personnel Training Model Research 2020 YB0464.

References

[1] M. Saraswat, K. Sharma, N. R. Chauhan, and R. K. Shukla, "Role of automation in energy management and distribution," *Journal of Scientific and Industrial Research*, vol. 79, no. 10, pp. 951–954, 2020.

[2] D. Xu, B. Wang, G. Zhang, G. Wang, and Y. Yu, "A review of sensorless control methods for AC motor drives," *CES Transactions on Electrical Machines And Systems*, vol. 2, no. 1, pp. 104–115, 2018.

[3] M. Dumitrescu, "Marine industry automation systems simulation," *Scientific Bulletin "Mircea cel Batran" Naval Academy*, vol. 22, no. 2, pp. 7–13, 2019.

[4] H. Chen, B. Jiang, and N. Lu, "A multi-mode incipient sensor fault detection and diagnosis method for electrical traction systems," *International Journal of Control, Automation and Systems*, vol. 16, no. 4, pp. 1783–1793, 2018.

[5] B. Pratap and S. Purwar, "Real-time implementation of nonlinear state and disturbance observer-based controller for twin rotor control system," *International Journal of Automation and Control*, vol. 13, no. 4, pp. 469–497, 2019.

[6] Y. Yuan, H. Yuan, D. W. C. Ho, and L. Guo, "Resilient control of wireless networked control system under denial-of-service attacks: a cross-layer design approach," *IEEE Transactions on Cybernetics*, vol. 50, no. 1, pp. 48–60, 2020.

[7] S. J. Gambhire, D. R. Kishore, P. S. Londhe, and S. N. Pawar, "Review of sliding mode based control techniques for control system applications," *International Journal of Dynamics And Control*, vol. 9, no. 1, pp. 363–378, 2021.

[8] O. V. Kryukov, I. V. Gulyaev, and D. Y. Teplukhov, "Method for stabilizing the operation of synchronous machines using a virtual load sensor," *Russian Electrical Engineering*, vol. 90, no. 7, pp. 473–478, 2019.

[9] M. S. Jansi and M. K. Elaiyarani, "Iot based home automation system," *Turkish Journal of Computer and Mathematics Education (TURCOMAT)*, vol. 11, no. 3, pp. 2246–2253, 2020.

[10] W. Liang, M. Zheng, J. Zhang et al., "WIA-FA and its applications to digital factory: a wireless network solution for factory automation," *Proceedings of the IEEE*, vol. 107, no. 6, pp. 1053–1073, 2019.

[11] C. Wei, M. Benosman, and T. Kim, "Online parameter identification for state of power prediction of lithium-ion batteries in electric vehicles using extremum seeking," *International Journal of Control, Automation and Systems*, vol. 17, no. 11, pp. 2906–2916, 2019.

[12] T. A. Skouras, P. K. Gkonis, C. N. Ilias, P. T. Trakadas, E. G. Tsampasis, and T. V. Zahariadis, "Electrical vehicles: current state of the art, future challenges, and perspectives," *Cleanroom Technology*, vol. 2, no. 1, pp. 1–16, 2019.

[13] Q. Shen, C. Yue, C. H. Goh, and D. Wang, "Active fault-tolerant control system design for spacecraft attitude maneuvers with actuator saturation and faults," *IEEE Transactions on Industrial Electronics*, vol. 66, no. 5, pp. 3763–3772, 2019.

[14] B. Xiang, X. Liu, and Y. Chen, "Event-based networked predictive control systems with secure transmission protocol," *International Journal of Control, Automation and Systems*, vol. 20, no. 4, pp. 1076–1086, 2022.

[15] M. Uzair, S. Yacoub Al-Kafrawi, K. Manaf Al-Janadi, and I. Abdulrahman Al-Bulushi, "A low-cost IoT based buildings management system (BMS) using arduino mega 2560 and raspberry pi 4 for smart monitoring and automation," *International Journal of Electrical and Computer Engineering Systems*, vol. 13, no. 3, pp. 219–236, 2022.

[16] W. Y. Choi, C. M. Kang, S. H. Lee, and C. C. Chung, "Radar accuracy modeling and its application to object vehicle tracking," *International Journal of Control, Automation and Systems*, vol. 18, no. 12, pp. 3146–3158, 2020.

[17] C. Yang, G. Peng, L. Cheng, J. Na, and Z. Li, "Force sensorless admittance control for teleoperation of uncertain robot manipulator using neural networks," *IEEE Transactions on Systems, Man, and Cybernetics: Systems*, vol. 51, no. 5, pp. 3282–3292, 2021.

[18] M. Zhang, Y. Zhang, and X. Cheng, "An enhanced coupling PD with sliding mode control method for underactuated double-pendulum overhead crane systems," *International Journal of Control, Automation and Systems*, vol. 17, no. 6, pp. 1579–1588, 2019.

[19] A. Benrabah, D. Xu, and Z. Gao, "Active disturbance rejection control of LCL-filtered grid-connected inverter using Padé approximation," *IEEE Transactions on Industry Applications*, vol. 54, no. 6, pp. 6179–6189, 2018.